Available online at www.sciencedirect.com

SciVerse ScienceDirect

Ceramics International 38 (2012) 4593–4599

CERAMICS INTERNATIONAL

www.elsevier.com/locate/ceramint

Photoluminescent properties of lead zirconate powders obtained by the polymeric precursor method

J.M.A. Nunes [a], J.W.M. Espinosa [b,*], M.F.C. Gurgel [c], P.S. Pizani [d], S.H. Leal [a], M.R.M.C. Santos [a], E. Longo [e]

[a] UFPI, Department of Chemistry, Campus Universitário Ministro Petrônio Portella, CEP: 64.049-550, Teresina, Piauí, Brazil
[b] UFG, Department of Industrial Engineering, Campus Catalão, CEP 75704-020, Catalão, Goiás, Brazil
[c] UFG, Department of Chemistry, Campus Jatai, CEP 75804-020, Jatai, Goiás, Brazil
[d] UFSCar, Department of Physics, CEP 13565-905, São Carlos, São Paulo, Brazil
[e] UNESP, Chemistry Institute, CEP 14801-970, Araraquara, São Paulo, Brazil

Received 19 January 2012; received in revised form 13 February 2012; accepted 14 February 2012
Available online 7 March 2012

Abstract

Lead zirconate powders, obtained by the polymeric precursor method, were annealed for 2 h at temperatures from 300 to 800 °C. The effect of heat treatment on structural defects and photoluminescent behavior was characterized by X-ray diffraction (XRD), Fourier transform infrared spectroscopy (FT-IR), Fourier transform Raman spectroscopy (FT-Raman), scanning electron microscopy (SEM), and photoluminescence spectroscopy (PL). XRD patterns and FT Raman spectra showed that the structure of the $PbZrO_3$ powders was orthorhombric. FT-IR spectra exhibited absorption bands at 450 and 860 cm^{-1}. These were ascribed to Zr–O bands and indicate the ZrO_6 octahedral group. SEM micrographs suggested that the annealing temperature allowed structural morphology changes in the samples. $PbZrO_3$ powders emitted green photoluminescence at room temperature and at lower annealing temperatures but no photoluminescence was observed from the ordered structure. This optical behavior was attributed to structural evolution from disordered to ordered as a function of $PbZrO_3$ powder annealing. The intensity of the green PL component increased after annealing at 300 °C.

Keywords: Powders; Chemical preparation; Optical properties; Perovskites; Characterization methods

1. Introduction

Perovskite-type compounds belong to a class of materials that have been investigated extensively since the 1940s due to their significance in fundamental research and high potential for technological applications [1]. The general formula of a perovskite compound is ABO_3 (where A = Ca, Sr, Pb or Ba and B = Ti or Zr). These are among the most important materials due to their electronic, ferroelectric and optical properties. Furthermore, they are some of the most versatile for chemical tuning of composition and structure. These materials display a plethora of physical and chemical properties of technological interest that depend on processing conditions, oxygen content, and order [1–6].

Interest in this kind of material is great because disordered semiconductors can replace single crystal semiconductors in many optoelectronic devices, especially regarding photoluminescent properties [7–11]. Our group has investigated a number of diverse structurally disordered materials, including the properties of perovskite-type compounds, such as $BaTiO_3$ [12], $CaTiO_3$ [13–15], $PbTiO_3$ [16,17], $BaZrO_3$ [18,19], $SrZrO_3$ [20] and $BaSrTiO_3$ [21].

Diverse theories in the literature indicate that the visible wide-band emissions observed in titanates belong to a universal green luminescence which is a characteristic property of practically all self-activated ABO_3 perovskite titanates [22]. Its origin has been explained and discussed in many papers. The mechanisms suggested in the literature include self-trapped excitons [23], recombination of electron and hole polarons and a charge transfer vibronic exciton [24], donor–acceptor recombination [25] and transitions in MeO_6 complexes [26].

The photoluminescent (PL) emission band of ABO_3 perovskites prepared by the polymeric precursor method is

* Corresponding author. Tel.: +55 64 3341 5328.
E-mail address: jowal98@hotmail.com (J.W.M. Espinosa).

0272-8842/$36.00
doi:10.1016/j.ceramint.2012.02.038

directly linked to the degree of structural order–disorder in the lattice, as well as to preparation method and thermal treatment conditions [27,28]. The optical properties of the amorphous semiconductors are dominated by the presence of an optical absorption tail that falls exponentially in the region and is usually transparent in crystalline solids. This is referred to as the absorption edge and is attributed to the presence of localized states in the typical band gap of amorphous semiconductors [29,30].

New studies describe the preparation and analysis of $Ba(Zr_xTi_{1-x})O_3$ (BZT) ceramic or thin films as a replacement for $BaTiO_3$. This is desirable since the Zr^{4+} ion is chemically more stable than the Ti^{4+} ion [31,32]. Recently, doped $PbZrO_3$ (PZT) has been chosen as an alternative material for the fabrication of ceramics and thin films by conventional solid state reaction and sol gel methods in order to analyze the antiferroeletric properties of this material [33,34].

In this study, $PbZrO_3$ (PZ) powders were synthesized by the polymeric precursor method (PPM), annealed at different temperatures (300–800 °C for 2 h) and analyzed to determine visible photoluminescence of amorphous and crystalline PZ powders at room temperature. The PZ powders were synthesized by soft chemical processing and analyzed by SEM, XRD, FT-IR, FT-Raman, PL spectra and PL curve decomposition into Gaussian peaks. The crystalline and disordered structures of the samples were confirmed by the previously mentioned techniques and corresponding photoluminescence properties were measured. Only the structurally disordered samples displayed visible PL at room temperature.

2. Experimental

PZ powders were prepared by the soft chemical polymeric precursor method (PPM) [35], Fig. 1. This process offers advantages over other synthesis techniques such as lower costs, better compositional homogeneity, higher purity, lower processing temperatures and the ability to coat larger substrate areas. In this method, zirconium citrates were formed by the dissolution of zirconium (IV) n-propoxide in an aqueous solution of citric acid at 60–70 °C.

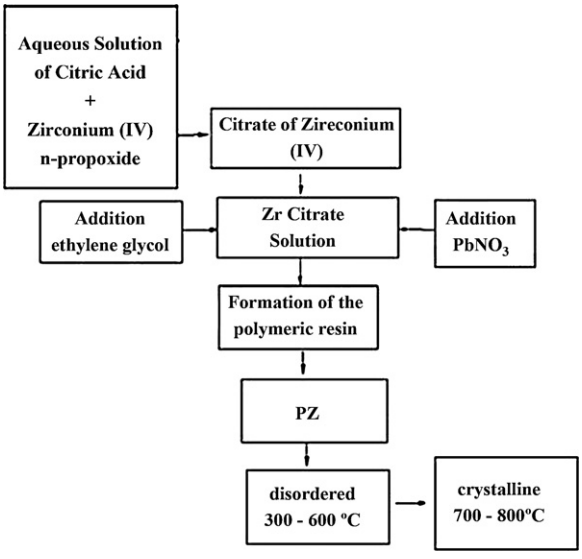

Fig. 1. General illustration of $PbZrO_3$ powder synthesis prepared by the polymeric precursor method.

After homogenization of the Zr solution, $PbNO_3$ was slowly added. In order to achieve total $PbNO_3$ dissolution, ammonium hydroxide was added drop by drop until the pH reached 7–8. Complete salt dissolution resulted in a clear solution. After complete dissolution of the $PbNO_3$ salt, ethylene glycol was added to promote polymerization of the mixed citrates by polyesterification. The molar ratio between the Pb and Zr cations was 1:1 and the citric acid/ethylene glycol ratio was fixed at 60/40 mass ratio. Heat treatment was carried out at various temperatures, from 300 to 800 °C for 2 h.

The PZ powders were structurally characterized by X-ray diffraction using a Rigaku D/Max-2400 diffractometer with Cu Kα radiation (λ = 1.5406 Å).

Infrared analysis was performed with an Equinox/55 (Bruker) Fourier transformed infrared (FT-IR) spectrometer. The FT-IR spectra of the powders were recorded at room temperature in the 400–3500 cm^{-1} frequency range, allowing observation of the lattice vibration at different temperatures.

Raman data was recorded using an RFS/100 Bruker FT-Raman spectrometer with a Nd:YAG laser producing a 1064.0 nm excitation light. Spectral resolutions of 4 cm^{-1} and 10–700 cm^{-1} were analyzed.

The PL spectra were recorded at room temperature with a U1000 Jobin-Yvon double monochromator coupled to a cooled GaAs photomultiplier and a conventional photon counter. The 488.0 nm excitation wavelength of an argon ion laser, set to maximum power output of 20 mW, was used. A cylindrical lens was used to prevent the sample from overheating and the slit width was 100 mm. All measurements were taken at room temperature. The dependence of grain morphology and size on annealing time was analyzed by scanning electronic microscopy using a DSM-940A Zeiss scanning electron microscope (SEM).

3. Results and discussion

3.1. X-ray diffraction

Fig. 2(a)–(f) shows the X-ray-diffraction patterns of all PZ powder samples annealed at 300, 400, 500, 600, 700 and 800 °C for 2 h. Fig. 2(a)–(c) illustrates the XRD patterns for these samples. Here the patterns are typical of disordered material indicating incomplete powder crystallization. In Fig. 2(c) and (d), the XRD patterns consist of peaks that are characteristic of crystalline PZ while the pattern in Fig. 2(f) is that of a polycrystalline material.

XRD patterns revealed that all PZ diffraction peaks could be indexed to the orthorhombic perovskite phase without secondary phases. This is in agreement with the ICDD card #490001. Relative intensities and sharp diffraction peaks indicate that the PZs are well-crystallized, suggesting long-range order. However the structurally ordered PZs clearly start at temperatures of 500 and 600 °C and are completely ordered

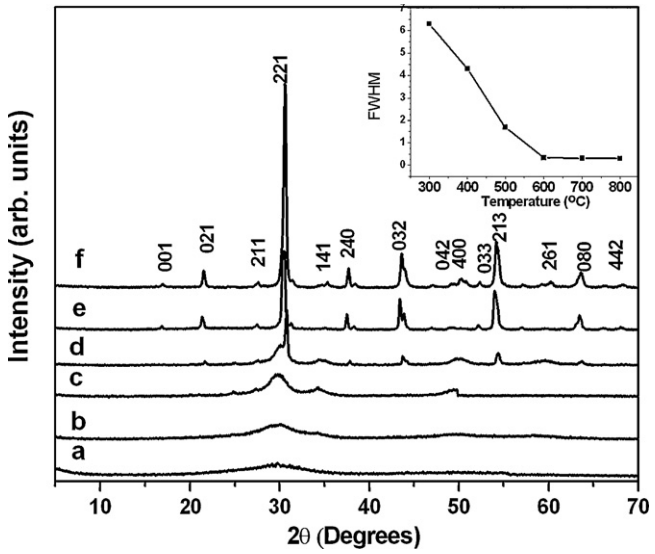

Fig. 2. XRD patterns of PZ powders for samples annealed at various temperatures (a) 300 °C, (b) 400 °C, (c) 500 °C, (d) 600 °C, (e) 700 °C and (f) 800 °C for 2 h. The figure inset shows FWHM analysis of the PZ powders.

after annealing at 800 °C. Fig. 2 shows decreasing full width half maxims (FWHM) until 600 °C. From 600 °C to 800 °C, FWHM behavior is constant. This fact characterizes the completely ordered PZ structure as long range.

3.2. FT-IR absorption spectra

The FT-IR absorption spectra of the PZ powders at 300, 400, 500, 600, 700 and 800 °C are shown in Fig. 3(a–f) respectively. Measurements were carried out in the transmission mode. In Fig. 3(a–d), representing disordered PZ, the infrared bands from 1558–1740 to 1190 cm^{-1} were associated with C–H, C–O and C–O–C stretching models, respectively.

Two peaks, one at 1696 cm^{-1} and the other at 1596 cm^{-1} demonstrate this fact and suggest that the Pb^{2+} ion is linked directly to the zirconium complex, affecting the carboxyls. These infrared bands are definite after heat treatment (see Fig. 3(e–f)). In Fig. 3(f), peaks in the spectrum at about 450, 750 and in the interval between 1500 and 1700 cm^{-1} demonstrate that polymerization of zirconium and lead nitrate occurs.

Inclusion of the lead atom leads to modification in the orientation of the metal planes in relation to the oxygen of the zirconium molecule and lead citrate, reinforcing the theory of lead as a network orientation. This suggests that, based on thermal analysis (not shown), the organic groups in the material completely decomposed at about 730 °C. Infrared absorption bands at 450 cm^{-1} and 860–530 cm^{-1} were associated with the Zr–O bonds that emerged after heat treatment at temperatures above 800 °C, suggesting the formation of ZrO_6 octahedra [36].

Characteristic vibration at about 730 cm was observed in the infrared absorption of the perovskite PZ crystalline. This is due to resonance with the optic (LO) phonon modes that become sharper and narrower and shift very slightly toward higher wave numbers. This is considered to be network stiffening and structural rearrangement, which leads to the perovskite phase formation and increased PZ crystallinity [37]

3.3. Raman spectra

Fig. 4 shows the Raman spectra of the room temperature PZ powder which is orthorhombic and belongs to the space group (*Pbam*). The PZ powder annealed at 300 °C maintains its amorphous nature. Powders annealed at higher temperatures result in the orthorhombic PZ perovskite phase. As a result, the Raman excitation of active modes becomes continually stronger, which is a good indication of crystalline development for the PZ perovskite phase at short-range order. The peaks at about 134, 205, 276, 338, 453, 498, 530 and 640 cm^{-1} are identified as $A_1(TO_1)$, $E(TO_2)$, $B_1 + E(TO)$, $A_1(TO_2)$, $E(LO_2) + A(LO_2)$, $E(TO_3)$, $E(TO_3)$ and $A_1(TO_3)$, respectively [36–38].

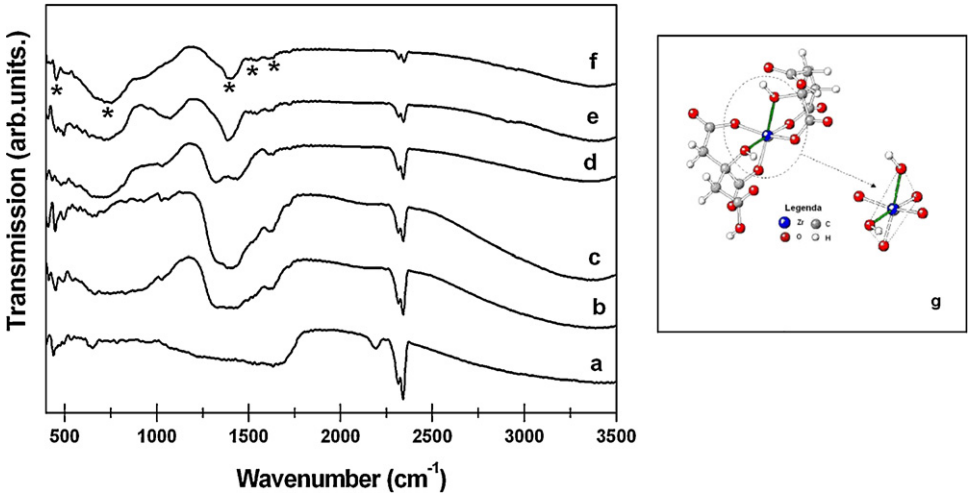

Fig. 3. FT-IR spectra of PZ powders annealed at various temperatures: (a) 300 °C, (b) 400 °C, (c) 500 °C, (d) 600 °C, (e) 700 °C, (f) 800 °C for 2 h and (g) complexation of carboxyls with zirconium ions to form the ZrO_6 octahedral.

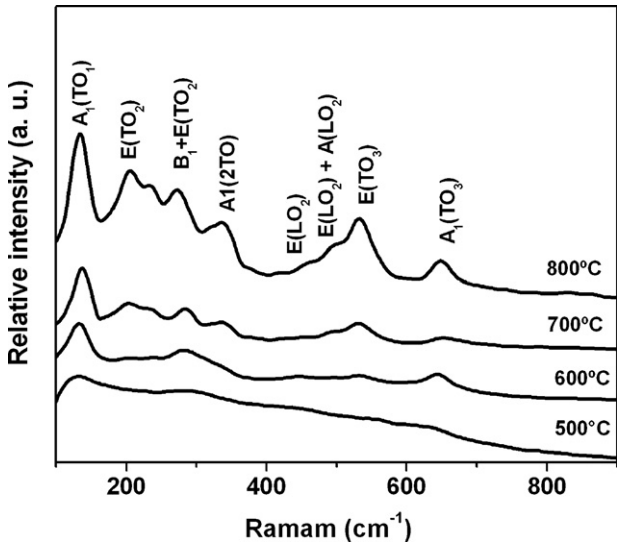

Fig. 4. Raman spectra at room temperature for PZ powders annealed at different temperatures (a) 300 °C, (b) 400 °C, (c) 500 °C, (d) 600 °C, (e) 700 °C and (f) 800 °C for 2 h.

3.4. PL spectra

Photoluminescence spectra of the PZ heat treated at 300, 400, 500 °C for 2 h are illustrated in Fig. 5(a–c), while the crystalline PZ, heat treated at 800 °C for 2 h can be seen in Fig. 5(d–f). The most general aspect of the spectra is a broad band covering a large part of the near visible spectra from 450 to 800 nm. All measurements were carried out at room temperature and the samples were excited by the 488 nm (2.54 eV) line of an argon laser. The PL spectra of the amorphous materials have a broad, intense band in the visible region with a maximum at about 580 nm. As observed in Fig. 5(d–f) the heat treatments at 600, 700 and 800 °C for 2 h produce material that does not produce any PL at room temperature. This behavior was observed in the ordered structure material. XRD, Raman spectra and FT-IR results confirm this PZ structural organization.

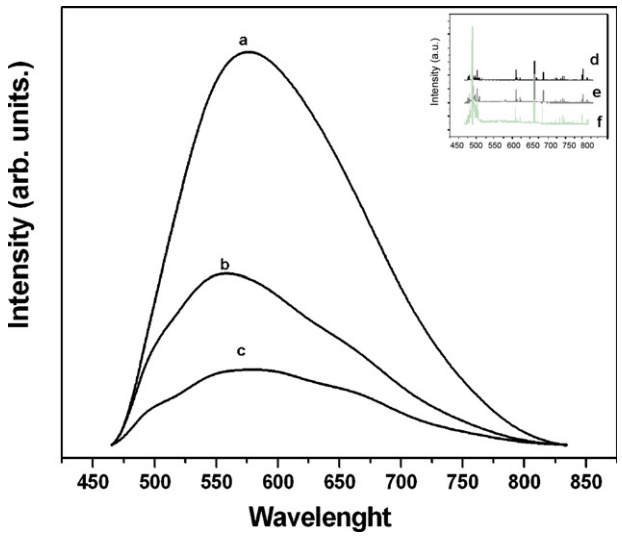

Fig. 5. Room-temperature PL spectra of PZ powder samples annealed at (a) 300 °C, (b) 400 °C, (c) 500 °C, (d) 600 °C, (e) 700 °C and (f) 800 °C for 2 h.

The photoluminescence phenomenon at room temperature occurs due to the structural disorder of the system. Therefore, if the system were totally ordered, PL would not exist. This disorder is characterized by the reduced band gap energy of the disordered PZ which leads to localized levels and an increase in the degeneracy of the valence (VB) and conduction (CB) bands. This structural disorder and the atomic orbitals of oxygen atoms in the intermediate GAP region lead to decreases in GAP which favors PL.

The disordered material is structured asymmetrically which could be related to the displacement of an atom of the perovskite ABO_3 material. According to Gurgel et al. [7,9] and their experimental studies correlated with quantum mechanical calculations, this asymmetry is responsible for the PL.

Therefore, during the annealing process, structure is completely disordered and is represented by network disorder seen in the powders annealed at 300, 400 and 500 °C network organization can be seen in the powders annealed at 600, 700 and 800 °C [39,40].

To clarify these concepts, two organization types were identified. The first one was a crystalline or ordered structure composed of the ideal $[ZrO_6–ZrO_6]$ and $[PbO_{11}–O–PbO_{11}]$ cluster networks. The second type consisted of a quasi-amorphous (ordered–disordered) structure containing networks of $[ZrO_5–O\cdots ZrO_6]$ and $[PbO_{11}–O\cdots PbO_{11}]$ clusters. These structural characteristics (ordered or disordered) come from the

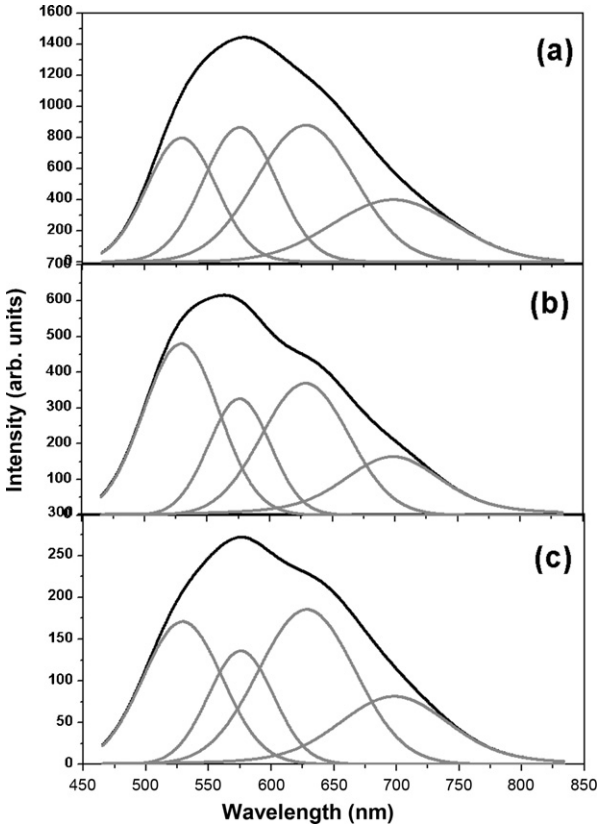

Fig. 6. Photoluminescence spectra decomposition of PZ powders annealed at: (a) 300 °C, (b) 400 °C and (c) 500 °C for 2 h.

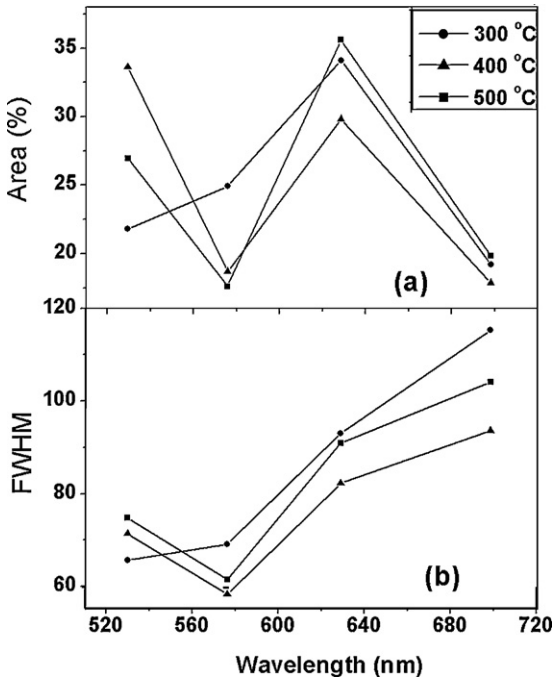

Fig. 7. (a) PL decomposition curve in Gaussian peaks and (b) Fourier decomposition/filtering algorithm.

short distance analysis and suggest that the material is asymmetrically structured.

3.5. PL curves (Peakfit decomposition)

In Fig. 6(a–c), broad, intense spectra in the visible green-yellow range (maximum below 575–580 nm) can be seen. Therefore, to better understand the PL properties and their dependence on the structural order–disorder of the lattice, these PL curves were investigated by Peakfit decomposition V4 [41,42]. The PL curves were analyzed by decomposition with a Gaussian response function and Fourier decomposition/filtering algorithm. The Gaussian line shape was successfully used to fit the PL peaks and can be seen in Fig. 6(a–b) for all PZ powders annealed for 2 h at: 300, 400 and 500 °C. PL curves for all samples are composed of four PL components: two bands called yellow components (peaks at 529.4 and 575.2 nm, respectively) and two red components (peaks at 628.5 and 698.2 nm). Each color represents a different type of electron transition and is linked to a specific structural arrangement.

3.6. PL decomposition curve in Gaussian peaks and Fourier decomposition/filtering

The PL decomposition curves in Gaussian peaks and Fourier decomposition/filtering algorithms are shown in Fig. 7(a and b).

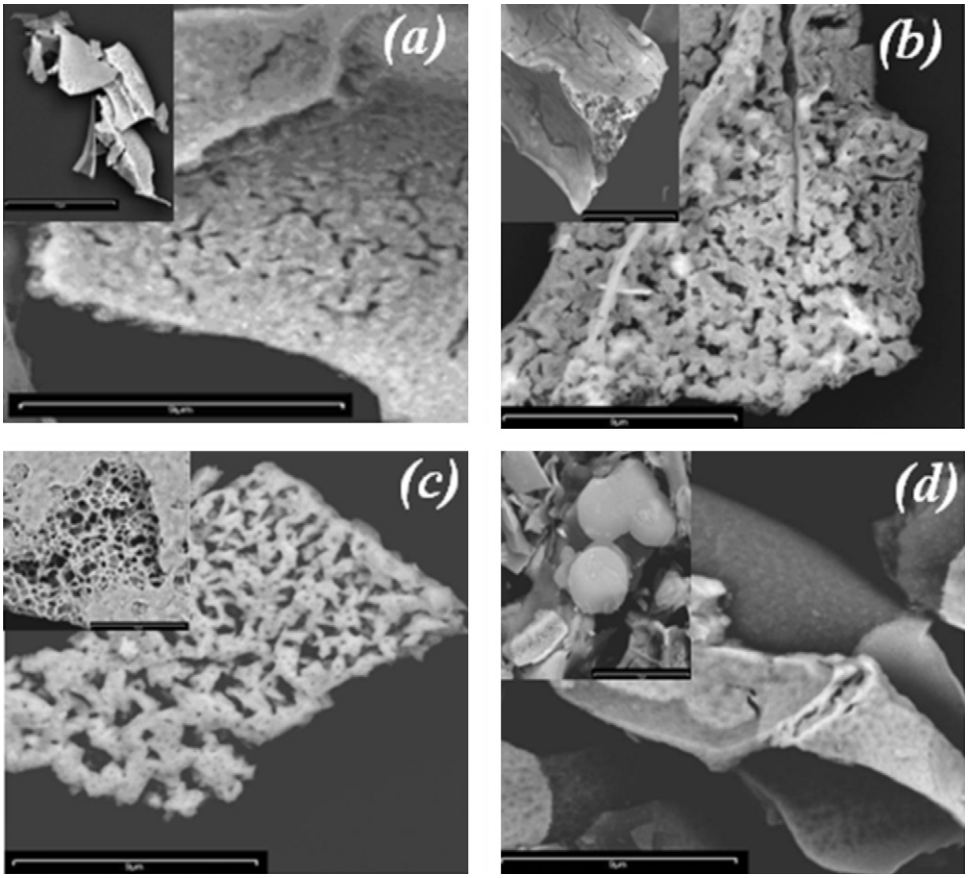

Fig. 8. Scanning electron micrographs of PZ annealed at (a) 500, (b) 600, (c) 700 and (d) 800 °C for 2 h.

Fig. 7(a) demonstrates that green PL intensity increased after annealing at 300 °C. At 500 °C, a higher percentage of red area was observed. This seems to indicate that the degree of structural order-disorder in this material is associated with annealing temperature such that higher temperatures lead to increases in structural order and consequent decreases in PL. Fig. 7(b) illustrates that for annealing temperatures above 600 °C, PL emissions decrease at excitation wavelengths of 488 nm and that at 800 °C PL intensity drops to virtually zero. This demonstrates high sample crystallinity (long-range order) and is in concordance with the XRD and Raman spectra. Higher PL intensity at 300 °C seems to indicate that this material has an optimum degree of structural order-disorder for photoluminescence. This may be associated with PZ results obtained during heat treatment, according to Raman results and particle size distribution.

3.7. Scanning electron microscopy

Fig. 8(a–d) shows PZ particle size and morphology measured by scanning electron microscopy for samples annealed at 500, 600, 700 and 800 °C for 2 h, respectively. This technique is very important for the analysis of powder surface morphology, since XRD is insufficient to characterize minor structural modifications and to draw meaningful correlations between PL response and structural changes in the sample [43,44]. This fact could be associated with defect concentrations arising from thermal treatment at 500, 600, 700 °C (see Fig. 8(a–c)) and 800 °C. Material ordering can be seen in Fig. 8(d).

4. Conclusions

Crystalline and disordered PZ powders were synthesized by PPM. SEM, X-ray diffraction, FT-IR, FT Raman, PL spectra and the PL decomposition curve in Gaussian peaks demonstrated that intermediate and short-range structural order-disorder defects can be generated by different annealing temperatures. Experimental measurements of the disordered powders suggested the presence of lattice defects. This powder is therefore intrinsically capable of producing PL at room temperature. The investigations also indicated that heat treatment leads to structural evolution from disorder to order. Ordered powders do not permit point defect creation. Consequently PL emissions were observed at room temperature but only at a specific level of order.

Acknowledgments

The authors are grateful for the financial support from the Brazilian research financing institutions: CNPq, CAPES, and FAPESP.

References

[1] M.E. Lines, A.M. Glas, Principles and Applications of Ferroelectrics and Related Materials, Clarendon, Oxford, 1977.
[2] H.I. Hsiang, C.S. Hsi, C.C. Huang, S.L. Fu, Sintering behavior and dielectric properties of $BaTiO_3$ ceramics with glass addition for internal capacitor of LTCC, J. Alloys Compd. 459 (2008) 307–310.
[3] V.V. Bannikov, I.R. Shein, V.L. Kozhevnikov, A.L. Ivanovskii, Magnetism without magnetic ions in non-magnetic perovskites $SrTiO_3$, $SrZrO_3$ and $SrSnO_3$, J. Magn. Magn. Mater. 320 (2008) 936–942.
[4] Y. Takahashi, T. Konishi, K. Soga, T. Fujiwara, Origin of hotoluminescence in suzukiite-type $BaTiSi_2O_7$, J. Ceram. Soc. Jpn. 116 (2008) 1104–1107.
[5] L. Luo, H.Z. Ren, X.G. Tang, C.R. Ding, H.Z. Wang, X.M. Chen, J.K. Jia, Z.F. Hu, Room temperature tunable blue-green luminescence in nanocrystalline. $(Pb_{1-x}Sr_x)TiO_3$ thin film grown on yttrium-doped zirconia substrate, J. Appl. Phys. 104 (2008), 043514-043514-5.
[6] A.Y. Liu, J.Q. Xue, X.J. Meng, J.L. Sun, Z.M. Huang, J.H. Chu, Infrared optical properties of $Ba(Zr_{0.20}Ti_{0.80})O^{-3}$ and $Ba(Zr_{0.30}Ti_{0.70})O^{-3}$ thin films prepared by sol–gel method, Appl. Surf. Sci. 254 (2008) 5660–5663.
[7] M.F.C. Gurgel, M.L. Moreira, E.C. Paris, J.W.M. Espinosa, P.S. Pizani, J.A. Varela, E. Longo, $BaZrO_3$ photoluminescence property: an ab initio analysis of structural deformation and symmetry changes, Int. J. Quant. Chem. 111 (2011) 694–701.
[8] S.R. Lazaro, J. Milanez, A.T. Figueiredo, V. Longo, V.R. Mastelaro, F.S. d e Vicente, A.C. Hernandes, J.A. Varela, E. Longo, Relation between photoluminescence emission and local order-disorder in the $CaTiO_3$ lattice modifier, Appl. Phys. Lett. 90 (2007) 111904–1111904.
[9] M.F.C. Gurgel, J.W.M. Espinosa, A.B. Campos, I.L.V. Rosa, M.R. Joya, A.G. Souza, J.A. Varela, E. Longo, Photoluminescence of crystalline and disordered BTO:Mn powder: experimental and theoretical modeling, J. Lumin. 126 (2007) 771–778.
[10] M.D. Gonçalves, L.S. Cavalcante, J.C. Sczancoski, J.W.M. Espinosa, P.S. Pizani, E. Longo, I.L.V. Rosa, $(Sr,Tm)ZrO_3$ powders prepared by the polymeric precursor method: synthesis, optical properties and morphological characteristics, Opt. Mater. (Amsterdam) 31 (2009) 1134–1143.
[11] S.C. Câmara, M.F.C. Gurgel, S.R. Lazaro, A. Beltràn, T.M. Boschi, E. Longo, Room temperature photoluminescence of the $Li_2ZnTi_3O_8$ spinel: experimental and theoretical study, Int. J. Quant. Chem. 71 (2004) 085113–085120.
[12] J.R. Sambrano, E. Orhan, M.F.C. Gurgel, A.B. Campos, M.S. Góes, C.O. Paiva - Santos, J.A. Varela, E. Longo, Theoretical analysis of the structural deformation in Mn doped $BaTiO_3$, Chem. Phys. Lett. 402 (2005) 491–496.
[13] V.S. Marques, L.S. Cavalcante, J.C. Sczancoski, D.P. Volanti, J.W.M. Espinosa, M.R. Joya, M.R.M.C. Santos, P.S. Pizani, J.A. Varela, E. Longo, Influence of microwave energy on structural and photoluminescent behavior of $CaTiO_3$ powders, Solid State Sci. 10 (2008) 1056–1061.
[14] M.L. Moreira, E.C. Paris, G.S. do Nascimento, V.M. Longo, J.R. Sambrano, V.R. Mastelaro, M.I.B. Bernardi, J. Andrés, J.A. Varela, E. Longo, Structural and optical properties of $CaTiO_3$ perovskite-based materials obtained by microwave-assisted hydrothermal synthesis: an experimental and theoretical insight, Acta Mater. 57 (2009) 5174–5185.
[15] J. Milanez, A.T. de Figueiredo, S.R. de Lazaro, V.M. Longo, R. Erlo, V.R. Mastelaro, R.W.A. Franco, E. Longo, J.A. Varela, The role of oxygen vacancy in the photoluminescence property at room temperature of the $CaTiO_3$, J. Appl. Phys. 106 (2009) 043526-1–043526-7.
[16] E.C. Paris, T.M. Boschi, M.R. Joya, P.S. Pizani, A.G. Souza, E.R. Leite, J.A. Varela, E. Longo, Investigation on the structural properties in Er-doped $PbTiO_3$ compounds: a correlation between experimental and theoretical results, J. Alloys Compd. 462 (2008) 157–163.
[17] M.F.C. Gurgel, E.C. Paris, J.W.M. Espinosa, C.O. Paiva-Santos, E.R. Leite, A.G. Souza, J.A. Varela, E. Longo, Jahn Teller effect on the structure of the Sm-doped $PbTiO_3$: a theoretical approach, J. Mol. Struct. Theochem. 813 (2007) 32–37.
[18] L.S. Cavalante, M.F.C. Gurgel, A.Z. Simões, M.R. Joya, E. Longo, J.A. Varela, P.S. Pizani, Intense visible photoluminescence in $Ba(Zr_{0.25}Ti_{0.75})O_3$ thin films, Appl. Phys. Lett. 90 (2007) 011901-1–011901-3.
[19] L.S. Cavalante, M.F.C. Gurgel, E.C. Paris, A.Z. Simões, M.R. Joya, J.A. Varela, P.S. Pizani, E. Longo, Combined experimental and theoretical investigations of the photoluminescent behavior of $Ba(Ti,Zr)O_3$ thin films, Acta Mater. (Oxford) 55 (2007) 6416–6426.

[20] V.M. Longo, L.C. Cavalcante, R. Erlo, V.R. Mastelaro, A.T. Figueiredo, J.R. Sambrano, S. de Lazaro, A.Z. Freitas, L. Gomes, N.D. Vieira Jr., E. Longo, Strong violet blue light photoluminescence emission at room temperature in $SrZrO_3$: joint experimental and theoretical study, Acta Mater. (Oxford) 56 (2008) 2191–2202.

[21] I.A. Souza, M.F.C. Gurgel, L.P.S. Santos, M.S. Góes, S. Cava, M. Cilense, I.L.V. Rosa, C.O. Paiva-Santos, E. Longo, Theoretical and experimental study of disordered $Ba_{0.45}Sr_{0.55}TiO_3$ photoluminescence at room, Chem. Phys. 322 (2006) 343–348.

[22] L. Jastrabik, S.E. Kapphan, V.A. Trepakov, I.B. Kudyk, R. Pankrath, Luminescence of $Ba_{0.77}Ca_{0.23}TiO_3$:Cr, J. Lumin. 102–103 (2003) 657–662.

[23] M. Aguilar, F. Agulló-López, X-ray induced processes in $SrTiO_3$, J. Appl. Phys. 53 (1982) 9009–9014.

[24] V.S. Vikhnin, R.I. Eglitis, S.E. Kapphan, E.A. Kotomin, G. Borstel, A new phase in ferroelectric oxides: the phase of charge transfer vibronic excitons, Europhys. Lett. 56 (2001) 702–708.

[25] E. Yamaichi, K. Watanabe, K. Ohi, The photoluminescence decay of the 2.2 eV-emission band in $KTaO_3$ single crystal, J. Phys. Soc. Jpn. 57 (1988) 2201–2206.

[26] G. Blasse, B.C. Grabmaier, Luminescent Materials, Springer-Verlag, Berlin, 1994.

[27] I.A. Souza, M.F.C. Gurgel, L.P.S. Santos, M.S. Góes, S. Cava, M. Cilense, I.L.V. Rosa, C.O. Paiva-Santos, E. Longo, Theoretical and experimental study of disordered $Ba_{0.45}Sr_{0.55}TiO_3$ photoluminescence at room temperature, Chem. Phys. 322 (2006) 343–348.

[28] L.S. Cavalcante, V.M. Longo, M. Zampieri, J.W.M. Espinosa, P.S. Pizani, J.R. Sambrano, J.A. Varela, E. Longo, M.L. Simões, C.A. Paskocimas, Experimental and theoretical correlation of very intense visible green photoluminescence in $BaZrO_3$ powders, J. Appl. Phys. 103 (8) (2008), 063527-063527-8.

[29] G.D. Cody, T. Tiedje, B. Abeles, B. Brooks, Y. Goldstein, Disorder and the optical-absorption edge of hydrogenated amorphous silicon, Phys. Rev. Lett. 47 (1981) 1480–1483.

[30] M. Capizzi, A. Frova, Optical gap of strontium titanate (deviation from urbach tail behavior), Phys. Rev. Lett. 25 (1970) 1298–1302.

[31] Y. Zhi, C. Ang, R. Guo, A.S. Bhalla, Dielectric properties and high tunability of $Ba(Ti_{0.7}Zr_{0.3})O_3$ ceramics under dc electric field, Appl. Phys. Lett. 81 (2002) 1285–1287.

[32] A. Dixit, S.B. Majumder, R.S. Katiyar, A.S. Bhalla, Relaxor behavior in sol–gel-derived $BaZr(0.40)Ti(0.60)O_3$ thin films, Appl. Phys. Lett. 82 (2003), 2679-2679-3.

[33] N. Vittayakorna, B. Boonchomd, Effect of $BiAlO_3$ modification on the stability of antiferroelectric phase in $PbZrO_3$ ceramics prepared by conventional solid state reaction, J. Alloys Compd. 509 (2011) 2304–2310.

[34] J. Parui, S.B. Krupanidhi, Effect of La modification on antiferroelectricity and dielectric phase transition in sol gel grown $PbZrO_3$ thin films, Solid State Commun. 150 (37–38) (2010) 1755–1759.

[35] M.P. Pechini, US Patent, 3330697 (1967).

[36] Y. Wang, J.J.S. Avilés, Synthesis of lead zirconate titanate nanofibres and the Fourier-transform infrared characterization of their metallo-organic decomposition process, Nanotechnology 15 (2004) 32–36.

[37] A.L.F. Osorio, A.V. Olmos, E.M. Zamora, J.M. Saniger, Preparation of free-standing $Pb(Zr_{0.52}Ti_{0.48})O_3$ nanoparticles by sol–gel method, J. Sol–Gel Sci. Technol. 42 (2007) 145–149.

[38] M. Deluca, T. Sakashita, W. Zhu, H. Chazono, G. Pezzotti, Stress dependence of the polarized Raman spectrum of polycrystalline lead zirconate titanate, J. Appl. Phys. 101 (2007) 083526-1–083526-12.

[39] V.M. Longo, L.C. Cavalcante, A.T. Figueiredo, L.P.S. Santos, E. Longo, J.A. Varela, J.R. Sambrano, C.A. Paskocimas, F.S. de Vicente, C. Hernandes, Highly intense violet-blue light emission at room temperature in structurally disordered $SrZrO_3$ powders, Appl. Phys. Lett. 90 (2007), 091906-091906-3.

[40] V.M. Longo, A.T. de Figueiredo, S. de Lazaro, M.F.C. Gurgel, G.S. Costa, C.O. Paiva-Santos, J.A. Varela, E. Longo, V.R. Mastelaro, F.S. de Vicente, A.C. Hernandes, R.W.A. Franco, Structural conditions that lead to photoluminescence emission in $SrTiO_3$: an experimental and theoretical approach, J. Appl. Phys. 104 (2008), 023515-023515-10.

[41] L.S. Cavalcante, J.C. Sczancoski, J.W.M. Espinosa, V.R. Mastelaro, A. Michalowicz, P.S. Pizani, F.S. De Vicente, M.S. Li, J.A. Varela, E. Longo, Intense blue and green photoluminescence emissions at room temperature in barium zirconate powders, J. Alloys Compd. 471 (2009) 253–258.

[42] T. Ding, W.T. Zheng, H.W. Tian, J.F. Zang, Z.D. Zhao, S.S. Yu, X.T. Li, F.L. Meng, Y.M. Wang, X.G. Kong, Temperature-dependent photoluminescence in $La_{2/3}Ca_{1/3}MnO_3$, Solid State Commun. 132 (2004) 815–819.

[43] X.J. Lou, J. Wang, Effect of manganese doping on the size effect of lead zirconate titanate thin films and the extrinsic nature of 'dead layers', J. Phys. Condens. Matter 22 (2010) 055901-1–055901-7.

[44] Y. Lin, C. Andrews, H.A. Sodano, Enhanced piezoelectric properties of lead zirconate titanate sol–gel derived ceramics using single crystal $PbZr_{0.52}Ti_{0.48}O_3$ cubes, J. Appl. Phys. 108 (2010) 06410-1–06410-6.